Journal of Alloys and Compounds 523 (2012) 139–145

Contents lists available at SciVerse ScienceDirect

Journal of Alloys and Compounds

journal homepage: www.elsevier.com/locate/jallcom

Synthesis and characterization of TiO_2/CdS core–shell nanorod arrays and their photoelectrochemical property

Chunlan Cao[a,b], Chenguo Hu[a,*], Weidong Shen[b], Shuxia Wang[a], Yongshu Tian[a,b], Xue Wang[a]

[a] Department of Applied Physics, Chongqing University, Chongqing 400044, PR China
[b] Department of Power Engineer, Chongqing Communication College, Chongqing 400035, PR China

ARTICLE INFO

Article history:
Received 16 December 2011
Received in revised form 14 January 2012
Accepted 22 January 2012
Available online 10 February 2012

Keywords:
TiO_2/CdS core–shell
Nanorod array
Hydrothermal method
Spin-coating

ABSTRACT

TiO_2/CdS core–shell nanorod arrays have been fabricated via a two-step method. Vertically aligned TiO_2 nanorod arrays (NRs) were synthesized by a facile hydrothermal method, and followed by depositing CdS nanoparticles on TiO_2 NRs by spin-coating successive ion layer adsorption and reaction (spin-SILAR) method. The surface morphology, structure, optical and photoelectrochemical behaviors of the core–shell NRs films are considered. The UV–vis absorption spectrum results suggested that the absorption peak of the TiO_2/CdS core–shell NRs shifts from the ultraviolet region to the visible region in comparison to that of the pure TiO_2 NRs. The obviously enhanced photoelectrochemical (PEC) performances of the heterojunction NRs were found under illumination of the simulated sunlight in comparison with that of the TiO_2 NRs. The enhanced PEC performance and formation mechanism of TiO_2/CdS core–shell NRs were discussed in detail.

1. Introduction

TiO_2 is one of the most promising materials in the photoelectrodes of light harvesting devices due to its excellent photocatalytic activity and facile synthetic routes for a variety of nanostructures, such as nanorods, nanotubes, nanobelts, and nanoparticles [1–7]. Aligned one-dimensional nanostructure arrays are beneficial to photovoltaic applications because they not only have ideal geometrical structures to provide a direct pathway for charge transport but also usually exhibit higher optical absorption cross-sections than thin films due to enhanced surface area, light scattering, and trapping abilities.

However, the optical quantum efficiency of TiO_2 under the irradiation of solar light is relatively low as it can only absorb the UV light (<387 nm), which is only 4–5% in the solar spectrum. A feasible method to solve this problem is to combine TiO_2 with narrow band gap semiconductors, but the energy band levels of the narrow band gap semiconductors must align well with those of TiO_2 so that the photoinduced electrons will transfer effectively to the collector electrode. Semiconductors such as CdS [8,9], CdSe [10,11], PbS [8,12], Bi_2S_3 [8,13], CdTe [14,15], and InP [16] have been widely used to improve the photoelectric response of TiO_2 in the visible region. Among these materials, nanocrystalline CdS is a direct band-gap semiconductor material with a reasonable band-gap of 2.4 eV which can effectively absorb the visible light. To date, CdS has been decorated on the TiO_2 system electrodes by different methods, such as electrochemical deposition [17–20] and sequential-chemical bath deposition (S-CBD) [21–24]. Recently, Zhang et al. [25] reported that uniform CdS/TiO_2 nanotube arrays could be fabricated by the method of successive ion layer adsorption and reaction (SILAR). However, the SILAR method is time-consuming and not easy to control, which requires a time-consuming rinsing step between the sequential adsorption processes for Cd^{2+} cations and S^{2-} anions in order to remove the excess ions from the surface. Without this rinsing step, the adsorption layer was uniform. Furthermore, the uniformity of the nanomaterials produced by the SILAR method was not reproducible because the technique depends on manual dipping and rinsing processes.

In this study, in order to overcome these problems, we report TiO_2/CdS core–shell nanorod arrays fabricated by a facile two-step, solution-based approach consisting of growth of TiO_2 NRs on transparent conductive glass (FTO) followed by successive ion layer adsorption and reaction (SILAR) for depositing CdS layers to form a shell. This method is based on spin-coating and is denoted spin-SILAR in order to distinguish it from the conventional SILAR method based on dip-coating (dip-SILAR). The spin-SILAR method involves a layer-by-layer buildup of a CdS film on TiO_2 surfaces via the successive adsorption and reaction of Cd^{2+} and S^{2-} by spin-coating. Because the adsorption, reaction, and rinsing steps occur simultaneously during spin-coating, spin-SILAR does not require rinsing steps, making the growth process simpler and faster than

* Corresponding author. Tel.: +86 23 65678362; fax: +86 23 65678362.
E-mail address: hucg@cqu.edu.cn (C. Hu).

0925-8388/$ – see front matter © 2012 Elsevier B.V. All rights reserved.
doi:10.1016/j.jallcom.2012.01.126

that of the dip-SILAR technique. The structural characteristics and optical properties of the as-prepared materials were characterized by FE-SEM, TEM, XRD, UV–vis absorption spectroscopy and photoluminescence spectroscopy. The photoelectric activity of the TiO_2/CdS core–shell NRs was evaluated and compared with pure TiO_2 NRs. The enhanced photoelectric property and formation mechanism of TiO_2/CdS core–shell NRs were discussed and illustrated.

2. Experimental

2.1. Materials

2.1.1. Preparation of TiO_2 NRs

The TiO_2 nanorod arrays was prepared using a hydrothermal synthesis reported previously [26]. Briefly, 10 mL of deionized water was mixed with 10 mL of concentrated hydrochloric acid (36 wt.% HCl). The mixture was stirred at ambient conditions for 5 min before 0.4 mL of titanium butoxide was added. After it was stirred for another 5 min, the mixture was placed in a Teflon-lined stainless steel autoclave of 25 mL volume. Then, one piece of FTO substrate, which has been cleaned for 10 min under action of ultrasonic wave in acetone, ethanol and deionized water, respectively, was placed at an angle against the wall of the Teflon liner with the conductive side facing down. The hydrothermal synthesis was conducted at 150 °C for 4 h in a furnace. After the synthesis, the FTO substrate was taken out and rinsed thoroughly with deionized water, ethanol and allowed to dry in ambient air.

2.2. Preparation of TiO_2/CdS core–shell nanorod arrays

The CdS nanoparticles (NPs) were deposited onto the TiO_2 NRs using the spin-SILAR method by dropping, sequentially, 1 mL of 50 mM $Cd(NO_3)_2$ and Na_2S solutions onto the samples followed by rotation at 1200 rpm for 20 s each time. The coating cycle ($Cd(NO_3)_2 \rightarrow Na_2S \rightarrow Cd(NO_3)_2 \rightarrow Na_2S$) without the water rinse step is termed as one cycle and the incorporated amount of CdS NPs can be increased by repeating the assembly cycles. For comparison, the same method is adopted to coat the CdS NPs on FTO (named CdS/FTO) repeated up to 20 cycles.

2.3. Characterization

The crystal structure of the samples was identified by XRD using Cu K_α radiation. The morphology, particle size and microstructure of the samples were examined by FE-SEM (FEI Nova 400, at 10 kV) and HRTEM (HRTEM 400 kV, JEOL4000EX). An UV–vis–NIR spectrophotometer (Hitachi U-4100) was used to measure the optical properties of the samples. Photoluminescence (PL) spectrum was performed with a HITACHI850-type visible–ultraviolet spectrophotometer with a Xe lamp as the excitation light source at room temperature. The excitation wavelength is 220 nm.

2.4. Photoelectrochemical measurement

The photocurrent densities were measured using a CHI660D workstation (CHI Co.), in a standard three-electrode configuration with the as-prepared samples as the working electrode, a Pt foil as the counter electrode, and a saturated calomel electrode (SCE) as the reference electrode, respectively, under irradiation of the simulated sunlight (CHF-XM-500 W) at intensity of 100 mW/cm^2. The light intensity was calibrated by a photometer (FZ-A). The electrolyte was 0.5 M Na_2SO_4 solution. The illuminated area of the working electrode is about 1.0 cm × 1.0 cm. All experiments were carried out under ambient conditions.

3. Results and discussion

3.1. Microstructure

Fig. 1 shows the morphological change before and after CdS deposition on the TiO_2 NRs. Fig. 1a and b shows typical FE-SEM images of the TiO_2 nanorod arrays at 150 °C for 4 h. The images reveal that the integral surface of the FTO substrate is covered with uniform TiO_2 NRs. Top and side views present the tetragonal ends of the nanorods with the highly ordered NRs. The inset of Fig. 1a represents a higher magnification of such arrays, showing that the nanorods are relatively smooth and nearly perpendicular to the FTO substrate. The vertically oriented TiO_2 NRs are around 6 μm in length, 50–80 nm in diameter. After deposition with CdS NPs for 20 cycles, the ordered TiO_2 NRs was retained, as shown in Fig. 1c and d. The images reveal the rough surface and dilated diameter of the TiO_2 nanorods in comparison with the uncoated nanorods, indicating that the CdS has been coated uniformly on the TiO_2 nanorods. Fig. 2(a)–(d) shows the TiO_2 NRs deposited with CdS NPs for different cycles from 5, 10, 15 and 20. Closer observation reveals that an increased amount of CdS NPs adsorbed on TiO_2 NRs accompanied the increase in spin-SILAR cycles. After 20 cycles of deposition, the entire surface of the TiO_2 NRs is covered with CdS NPs (inset of Fig. 1(c)). EDS was applied to determine the composition of the nanostructure. The EDS spectra collected from pure TiO_2 and TiO_2/CdS core–shell NRs are shown in Fig. 1e and f. While EDS spectrum (Fig. 1e) reveals the existence of O and Ti elements (Sn and Si peaks are from the substrate), suggesting that NRs are pure TiO_2. Cd and S elements are found in the CdS coated TiO_2 nanorods with the atomic ratio of Ti, O, Cd and S is 17.99, 64.47, 5.67 and 5.64%, respectively, demonstrating the successful coating of CdS nanoparticles on the surface of TiO_2 nanorods.

Detailed morphological features and crystallinity of the TiO_2 and TiO_2/CdS core–shell nanostructures were investigated using TEM and selected area electron diffraction (SAED) analyses as shown in Fig. 3. Fig. 3a shows TEM image of TiO_2 nanorods, confirming the smooth surface of the nanorods. And Fig. 3b is the corresponding SAED pattern, which is in consistent with the tetragonal rutile phase (JCPDS card No. 89-4920). The nanorods grow along [0 0 1] direction. The TEM image of the TiO_2/CdS (Fig. 3c and d) nanostructure shows that the high-density CdS nanoparticles are uniformly bonded to the surface of the TiO_2 nanorod.

3.2. XRD analysis

The crystal structure of the TiO_2/CdS core–shell NRs (pattern c) was examined by X-ray diffraction (XRD) experiments as shown in Fig. 4. For comparison, XRD patterns from the pure TiO_2 NRs (pattern b) and FTO substrate (pattern a) are also given. All diffraction peaks in pattern b can be well indexed by the tetragonal rutile phase of TiO_2 (JCPDS file No. 89-4920, marked by ▲). The crystallization of the TiO_2 NRs is in agreement with that shown in the SAED pattern in Fig. 3b. CdS peaks in pattern c reveal that the CdS has been actually coated on the TiO_2 with the cubic structure (JCPDS file No.10-0454, marked by △). The X-ray diffraction pattern also confirms that no significant Cd- or S-related impurities are present in the TiO_2/CdS core–shell NRs.

3.3. Optical analysis

Fig. 5a shows the UV–vis transmittance spectra of the pure TiO_2 NRs, CdS/FTO and TiO_2/CdS core–shell NRs after deposition with CdS NPs for 20 cycles. It can be seen that pure TiO_2 NRs and CdS NPs absorbed in the UV region with a band edge ~386 nm and ~530 nm (2.35 eV), respectively, on the other hand, the absorption edge of TiO_2/CdS core–shell NRs composite falls into the visible region at the wavelength of 483 nm and it is red-shifted about 100 nm in comparison with that of pure TiO_2 NRs demonstrating that the absorption spectrum of TiO_2 NRs can be sensitized with CdS NPs. The band gap of CdS is about 2.45 (505 nm) with zinc blende structure [27]. Here, the absorption edge reveals the band gap of the CdS coated on the TiO_2 is about 2.56 eV (483 nm). The enlarged band gap attributes to the quantum size effect caused by the small particle size of CdS on the TiO_2 NRs. The heterojunction of TiO_2/CdS core–shell structure can efficiently absorb the sunlight.

The PL spectra have been widely used to investigate the transfer behavior of the photogenerated electrons and holes in semiconductor materials. It can reflect the separation and recombination of

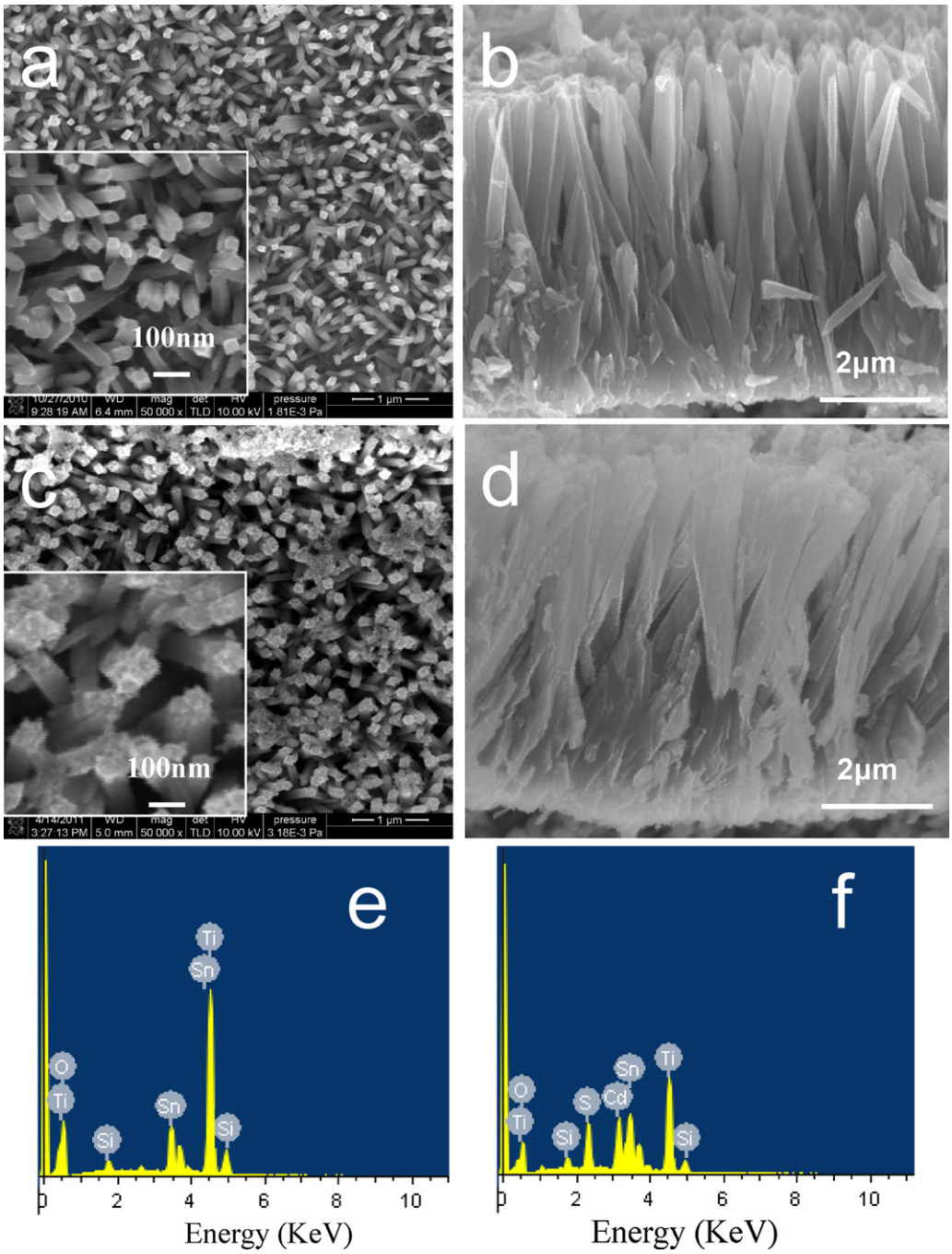

Fig. 1. FESEM images of top view (a) and side view (b) of the pure TiO_2 NRs grown on FTO; top view (c) and side view (d) of the TiO_2/CdS core–shell nanorod heterostructure arrays (after deposition with CdS NPs for 20 cycles). Insets are the corresponding larger magnification images. EDS recorded from the pure TiO_2 NRs (e) and TiO_2/CdS core–shell nanorod heterostructure arrays (f).

photogenerated electron–hole pairs [28], and the structure information as well. Fig. 5(b) shows the PL spectra of the pure TiO_2 and TiO_2/CdS core–shell NRs with an excitation wavelength of 220 nm. It can be seen that the pure TiO_2 NRs shows an obvious peak A at 357 nm (3.49 eV) and peak B around 403 nm (3.08 eV). The emission around 3.49 eV corresponds to the near band edge emissions of the nanostructured TiO_2, while the peak B around 3.08 eV may originate from the charge recombination on the shallow-trap surface states. Peak B is stronger than peak A, indicating lots of defects on the TiO_2 nanorods. However, the near band edge emission A of the TiO_2 NRs is greatly enhanced, while the emission B from the charge recombination on the shallow-trap surface states of the pure TiO_2 NRs disappears owing to the defect passivation by coating the CdS. We have also seen a new broad peak C centered at 525 nm, which partially attributes to the recombination of photogenerated electron–hole pairs within CdS as a result of a little thick accumulation of CdS nanoparticles on the top of the TiO_2 nanorods, and partially attributes to the recombination of the transferred electrons on the conduction band of TiO_2 with the holes on the valence band of CdS. Anyhow, the great enhancement of peak A for the TiO_2/CdS core–shell NRs implies that charge separation occurs before the recombination within CdS.

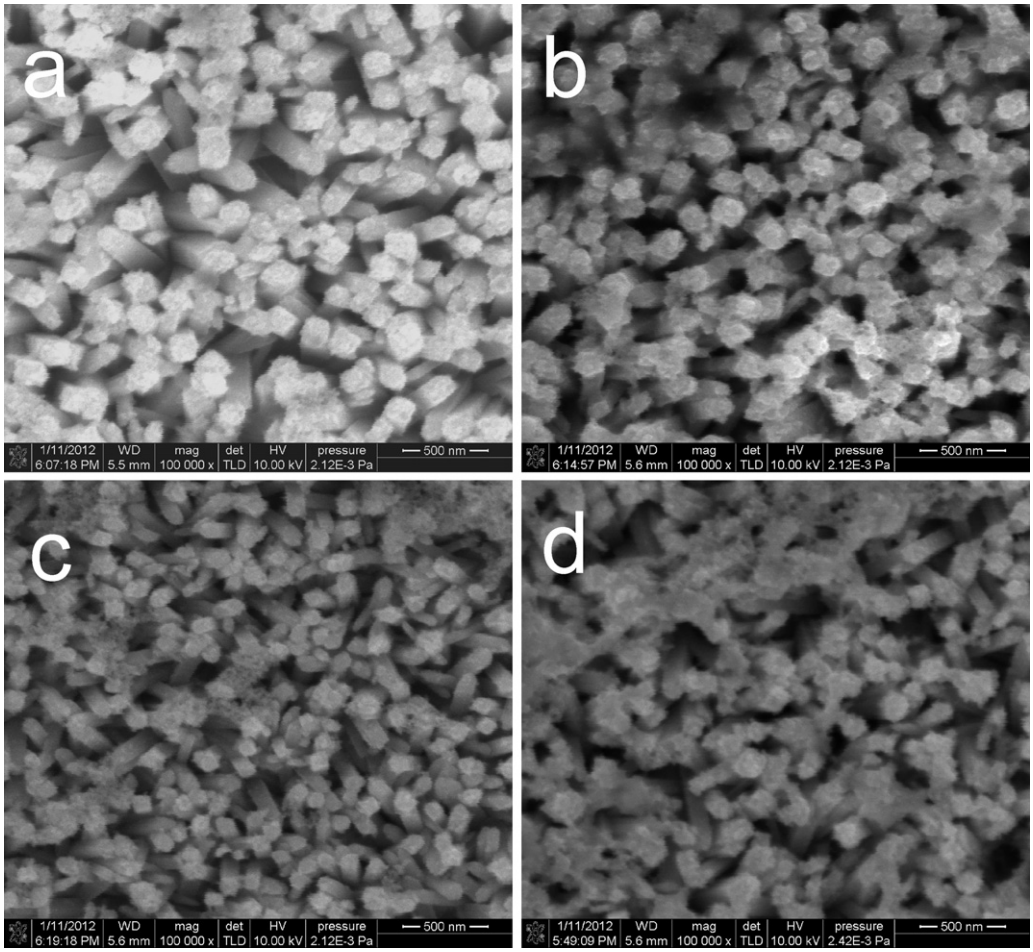

Fig. 2. FESEM images of top view of the TiO_2 NRs after introduction of 5 cycles (a), 10 cycles (b), 15 cycles (c) and 20 cycles (d) by the spin-SILAR process for incorporation of CdS NPs.

3.4. Photoelectrochemical characterization

Photoelectrochemical properties of the pure TiO_2, CdS/FTO and TiO_2/CdS core–shell NRs were evaluated by employing the three electrodes, respectively, in a photoelectrochemical cell containing Na_2SO_4 (0.5 M solution) as an electrolyte. The responses of the different anodes under intermittent illumination are shown in Fig. 6a. Such measurements are indicative of the reproducibility of photoresponses. The three electrodes show an instantaneous change in current upon illumination. The current retract to original values almost instantaneously once the illumination is switched off. This trend is repeated with every on–off cycle (labeled in Fig. 6a). We found that photoelectrochemical properties could be dramatically enhanced by using TiO_2/CdS core–shell NRs as the electrode, comparing with pure TiO_2 NRs and CdS/FTO. The photocurrent density produced by TiO_2/CdS core–shell NRs film electrode reached 80.2 $\mu A\,cm^{-2}$. This value was about 2.0 times of that by CdS/FTO electrode and 5 times of that by pure TiO_2 NRs film electrode, respectively. The photoelectrochemical performances of the samples were further investigated by linear-sweep photovoltammetry under the simulated sunlight irradiation as is shown in Fig. 6b. The dark-current densities of these samples were found to be negligible. Curve d in Fig. 6b indicates that the TiO_2 NRs sensitized by the CdS NPs can enhance the photoelectrochemical activity under visible light, with the generated maximum photocurrent increasing from 10 $\mu A\,cm^{-2}$ for TiO_2 to 26.8 $\mu A\,cm^{-2}$ for TiO_2/CdS core–shell NRs, about 2.68 times of increase. This dramatic photoelectrochemical performance enhancement may be attributed to the following reasons: (1) the extension of absorption spectrum into the visible region by TiO_2/CdS core–shell NRs film electrodes; (2) an improvement of charge separation; (3) the reduction of recombination rate of electron–hole; (4) an increase in the lifetime of the charge carrier and (5) an enhancement of the interfacial charge transfer efficiency to adsorbed substrate [29].

Michael Grätzel has reported that the both conduction band (CB) and valence band (VB) position of CdS (−0.52 eV, 1.88 eV) are above to those of TiO_2 (−0.29 eV, 2.91e V) vs. NHE (pH = 0) [30]. According to band positions, we drew the schematic diagram to explain the enhanced photoelectric current for the TiO_2/CdS core–shell NRs as indicated in Fig. 7. In aqueous solution, Na_2SO_4 forms OH^-, Na^+ and HSO_4^- (Eq. (1)). Because the conduction band bottom of CdS is above that of the TiO_2, when CdS is combined with TiO_2, local band bending occurs at the CdS/TiO_2 interface and a local electric field is established. When illuminated, CdS can effectively absorb visible light and excite electrons and holes pairs (Eq. (2)). The TiO_2 nanorods can also produce photogenerated electron–hole pairs as the CdS was not fully coated on the whole nanorods. The local electric field at the CdS/TiO_2 interface pushes the photongenerated electrons from CB of CdS to the CB of TiO_2 and holes from TiO_2 to VB of CdS (Eq. (3)). Under the light illumination, the photogenerated electrons transformed from TiO_2 NRs to barrier layer and then to FTO (Eq. (4)) and ultimately to Pt foil (Eq. (5)) through

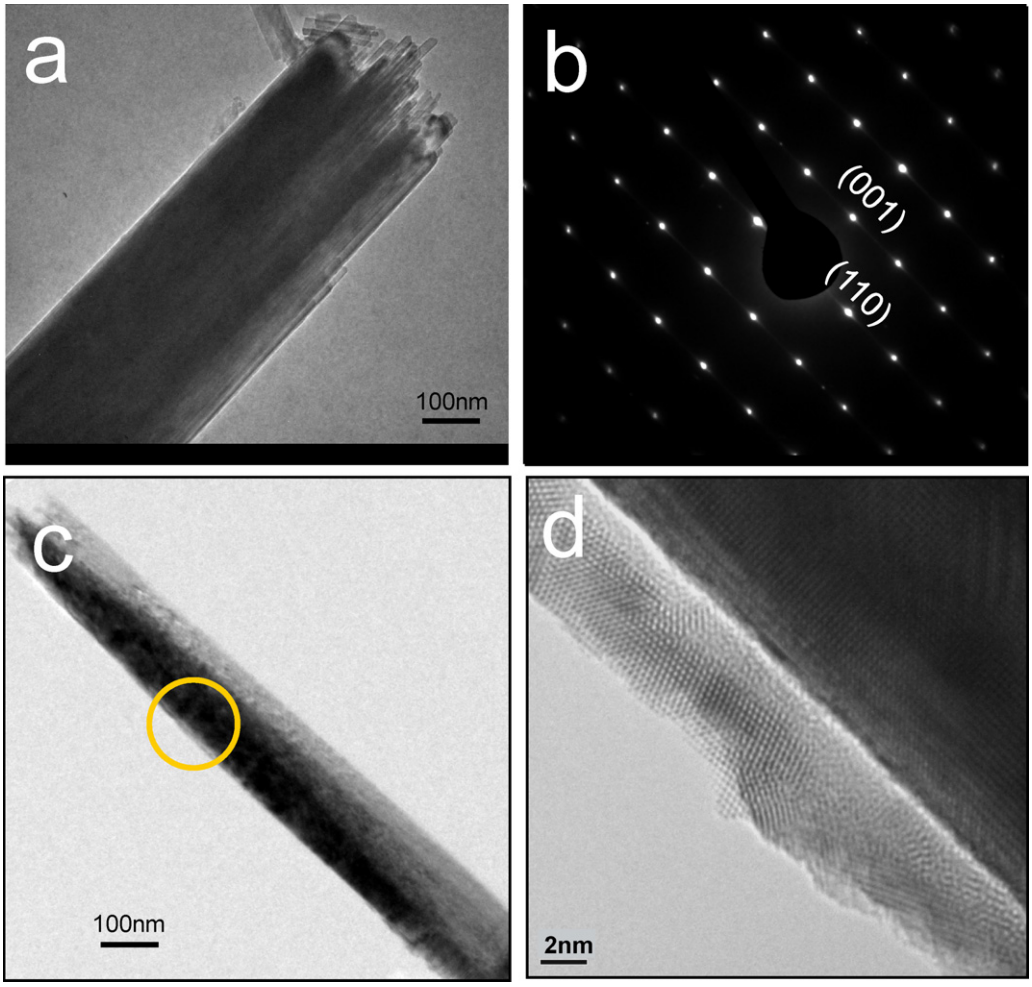

Fig. 3. TEM image (a) and SAED pattern (b) of TiO_2 nanorods. TEM image of a low (c) and high (d) magnification of the TiO_2/CdS core–shell nanorod (after deposition with CdS NPs for 20 cycles).

external circuit. Consequently, the photogenerated electrons are scavenged by hydrogen ion on the Pt foil, forming hydrogen gas [31–34] (Eq. (6)), while the photogenerated hole moved to the TiO_2/CdS core–shell NRs/electrolyte interface and were collected by the hole scavengers (SO_4^{2-}) (Eq. (7)). Therefore, the efficiency

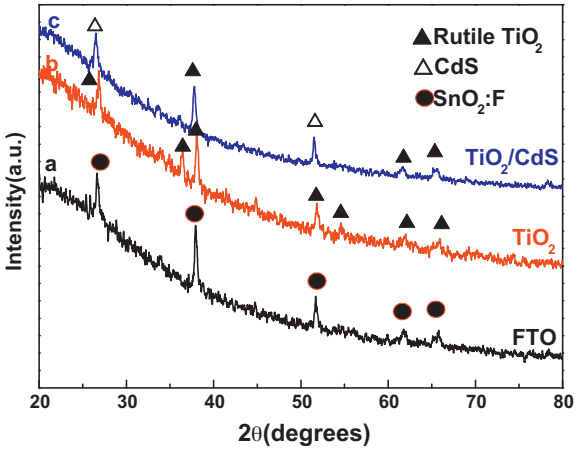

Fig. 4. XRD of FTO substrate (a), pure TiO_2 NRs (b) and TiO_2/CdS core–shell nanorod heterostructure arrays (after deposition with CdS NPs for 20 cycles) (c).

can be assessed by monitoring the photocurrent with respect to the active area of the photoanode. Major reactions that occur in this system can be summarized as follows:

$$H_2O + Na_2SO_4 \rightarrow (Na^+OH^-) + (Na^+HSO_4^-) \quad (1)$$

$$CdS + h\nu \rightarrow CdS(e^- + h^+)(\text{electron–hole} \rightarrow \text{separation}) \quad (2)$$

$$CdS(e^- + h^+) + TiO_2 \rightarrow CdS(h^+) + TiO_2(e^-) \quad (3)$$

$$TiO_2(e^-) \rightarrow TiO_2 + FTO(e^-) \quad (4)$$

$$FTO(e^-) \rightarrow Pt(e^-) + FTO \quad (5)$$

$$Pt(e^-) + 2H^+ \rightarrow Pt + H_2 \quad (6)$$

$$CdS(h^+) + 2HSO_4^- \rightarrow CdS + 2SO_4^{2-} + 2H^+ \quad (7)$$

3.5. Mechanism analysis

Based on the experimental results mentioned above, the growth mechanism of the TiO_2/CdS core–shell nanorod heterostructure arrays can be proposed tentatively. Firstly, the dissolved $Cd(NO_3)_2{\cdot}4H_2O$ in deionized water produces cadmium ion (Eq. (8)) and the dissolved $Na_2S{\cdot}9H_2O$ can generate free sulfide ion (Eq. (9)), so that this experiment was conducted for 20 s at 1200 rpm between alternating spin-coating applications of Cd^{2+} or S^{2-}. Secondly, when the dissolved $Cd(NO_3)_2{\cdot}4H_2O$ is dropped on the TiO_2

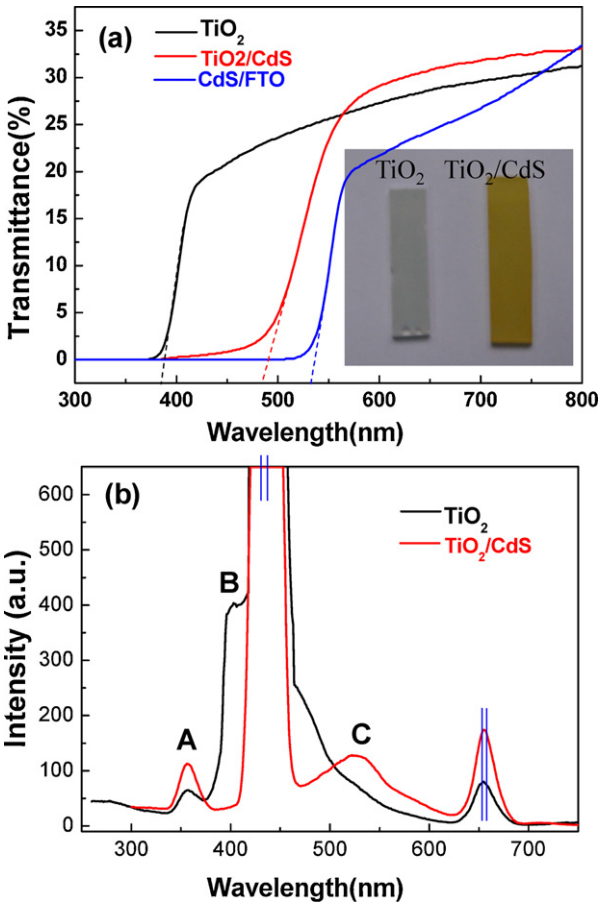

Fig. 5. UV–visible light transmittance (a) and photoluminescence (PL) emission spectra (b) of the as-prepared pure TiO_2 and TiO_2/CdS core–shell NRs (after deposition with CdS NPs for 20 cycles). Inset: photograph of TiO_2 and TiO_2/CdS films.

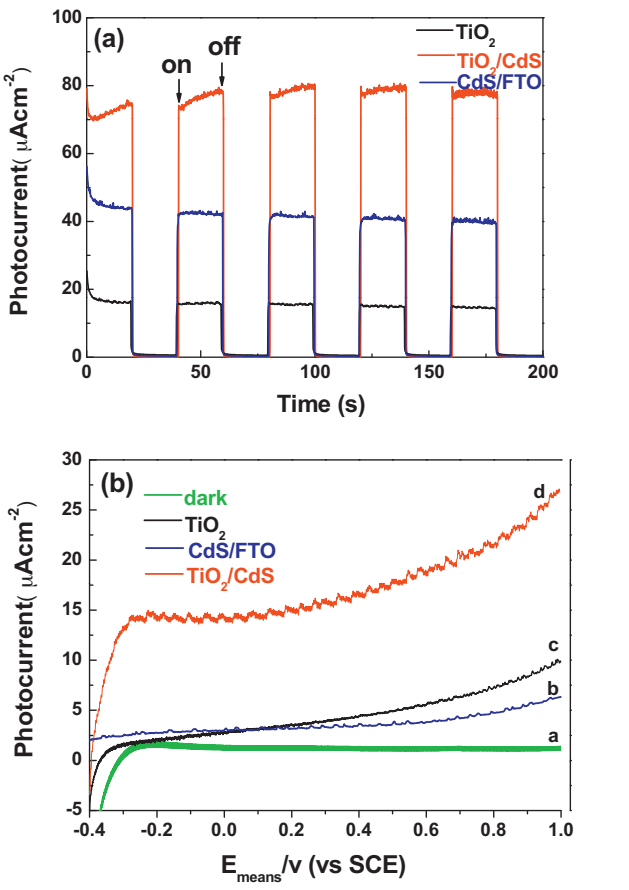

Fig. 6. (a) Photocurrent responses in 0.5 M Na_2SO_4 solution for the TiO_2 and TiO_2/CdS NRs electrodes (after deposition with CdS NPs for 20 cycles) under radiation of 100 mW cm^{-2} simulated sunlight, (b) photocurrent vs. potential curves for thin film electrodes of TiO_2 and TiO_2/CdS NRs (after deposition with CdS NPs for 20 cycles) in 0.5 M Na_2SO_4 electrolyte under the visible-light illumination (100 mW cm^{-2}). The electrode area was 1.0 cm × 1.0 cm and the scan rate was 100 mV/s.

NRs, cadmium ion can easily deposit on the surface of TiO_2 NRs. Finally, the cadmium ion can be changed to CdS (Eq. (10)) through an ion-by-ion mechanism [35] by the generated and dissolved sulfide ion in aqueous solution at room temperature. Such cycle-dependent ion-by-ion growth in the solution-phase SILAR process is analogous to vapor-phase atomic layer deposition (ALD), which is a very powerful thin film growth technique in current semiconductor processing.

$$Cd(NO_3)_2 \rightarrow Cd^{2+} + 2NO_3^- \quad (8)$$

$$NaS \rightarrow 2Na^+ + S^{2-} \quad (9)$$

$$Cd^{2+} + S^{2-} \rightarrow CdS \quad (10)$$

Depending on the geometry of the TiO_2 NRs, CdS shell coating occurs mainly on the tip (Fig. 8) or on the lateral surfaces of the aligned TiO_2 nanorods. It is found that the chemical concentration of the solution can affect the CdS deposition rates. Thus, a uniform CdS shell coats on the surface via the successive adsorption/absorption and reaction of Cd^{2+} and S^{2-} by spin-coating. However, in the case of the high-density aligned TiO_2 NRs, the space between nanorods is very small. This tiny/minute space hinders the mass transport of the reactants through it to the bottom of the array, and thus these effects cause CdS shell coating mainly to proceed on the upper part of the nanorods. The whole process is shown in Fig. 8.

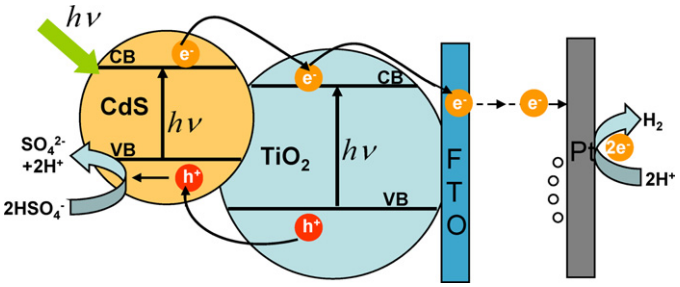

Fig. 7. Schematic diagram of the TiO_2/CdS core–shell NRs electrodes and Pt cathode, showing the band-gap alignment, electron–hole generation and separation, charge transport, and generating of hydrogen.

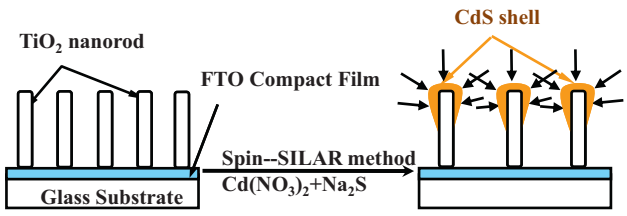

Fig. 8. Schematic illustration for the construction of the TiO_2/CdS core–shell nanorod heterostructure arrays.

4. Conclusions

TiO_2/CdS core–shell nanorod arrays with visible light activity have been prepared by a two-step method. The CdS coating can effectively compensate defects on the surface of TiO_2 nanorods. The TiO_2/CdS NRs obviously increases the visible-light absorption compared with the pure TiO_2 NRs. The TiO_2/CdS NRs induces the shift of the absorption edge into the visible-light range due to the narrowing of the band gap. The TiO_2 NRs coated by CdS nanoparticles show higher photocurrent value than that of pure TiO_2 NRs. The enhanced PEC behaviors can be attributed to the coated CdS, which increases the probability of electron–hole separation and extends the range of the TiO_2 photoresponse from ultraviolet to visible region due to the low band gap of 2.56 eV. The approach to obtain the TiO_2/CdS NRs described in this study is novel and feasible.

Acknowledgments

This work is supported by the NSFC (60976055), SRFDP (20110191110034), Project (WLYJSBJRCTD201101) of the Innovative Talent Funds for 985 Project, and the large-scale equipment sharing fund of Chongqing University.

References

[1] G.K. Mor, K. Shankar, M. Paulose, O.K. Varghese, C.A. Grimes, Nano Lett. 5 (2005) 191–195.
[2] S.E. John, S.K. Mohapatra, M. Misra, Langmuir 25 (2009) 8240–8247.
[3] N.K. Allam, C.A. Grimes, Langmuir 25 (2009) 7234–7240.
[4] Y.B. Xie, Electrochim. Acta 51 (2006) 3399–3406.
[5] S. Pokhrel, L.H. Huo, H. Zhao, S. Gao, Sens. Actuators B 129 (2008) 18–23.
[6] Y.S. Tian, C.G. Hu, X.S. He, C.L. Cao, G.S. Huang, K.Y. Zhang, Sens. Actuators B 144 (2010) 203–207.
[7] T. Kawahara, Y. Konishi, H. Tada, N. Tohge, J. Nishii, S. Ito, Angew. Chem. Int. Ed. 41 (2002) 2811.
[8] R. Vogel, P. Hoyer, H. Weller, J. Phys. Chem. 98 (1994) 3183–3188.
[9] S. Banerjee, S.K. Mohapatra, P.P. Das, M. Misra, Chem. Mater. 20 (21) (2008) 6784–6791.
[10] Q. Shen, T. Sato, M. Hashimoto, C. Chen, T. Toyoda, Thin Solid Films 499 (2006) 299–305.
[11] J. Hensel, G. Wang, Y. Li, Y. Jin, Z. Zhang, Nano Lett. 10 (2010) 478–483.
[12] R. Plass, S. Pelet, J. Krueger, M. Gratzel, J. Phys. Chem. B 106 (2002) 7578–7580.
[13] L.M. Peter, K.G.U. Wijayantha, D.J. Riley, J.P. Waggett, J. Phys. Chem. B 107 (2003) 8378–8381.
[14] J.A. Seabold, K. Shankar, R.H.T. Wilke, M. Paulose, O.K. Varghese, C.A. Grimes, K.S. Choi, Chem. Mater. 20 (2008) 5266–5273.
[15] X.F. Gao, H.B. Li, W.T. Sun, Q. Chen, F.Q. Tang, L.M. Peng, J. Phys. Chem. C 113 (2009) 7531–7535.
[16] J.L. Blackburn, D.C. Selmarten, R.J. Ellingson, M. Jones, O. Micic, A.J. Nozik, J. Phys. Chem. B 109 (2005) 2625–2631.
[17] S.G. Chen, M. Paulose, C. Ruan, G.K. Mor, O.K. Varghese, D. Kouzoudis, C.A. Grimes, J. Photochem. Photobiol. A: Chem. 177 (2006) 177–184.
[18] Y.X. Yin, Z.G. Jin, F. Hou, Nanotechnology 18 (2007) 495608.
[19] C.L. Wang, L. Sun, H. Yun, J. Li, Y.K. Yue, C.J. Lin, Nanotechnology 20 (2009) 295601.
[20] C.L. Wang, S. Lan, K.P. Xie, C.J. Lin, Sci. China Ser. B: Chem. 52 (2009) 2148–2155.
[21] W.T. Sun, Y. Yu, H.Y. Pan, X.F. Gao, Q. Chen, L.M. Peng, J. Am. Chem. Soc. 130 (2008) 1124–1125.
[22] D.R. Baker, P.V. Kamat, Adv. Funct. Mater. 19 (2009) 805–811.
[23] C.J. Lin, Y.T. Lu, C.H. Hsieh, S.H. Chien, Appl. Phys. Lett. 94 (2009) 113102.
[24] X.W. Zhang, L.C. Lei, J.L. Zhang, Q.X. Chen, J.G. Bao, B. Fang, Sep. Purif. Technol. 66 (2009) 417–421.
[25] J. Zhang, C. Tang, J.H. Bang, Electrochem. Commun. 12 (2010) 1124–1128.
[26] C. Cao, C. Hu, X. Wang, S. Wang, Y. Tian, H. Zhang, Sens. Actuators B: Chem. 156 (2011) 114–119.
[27] K.S. Ramaiah, R.D. Pilkington, A.E. Hill, R.D. Tomlinson, A.K. Bhatnagar, Mater. Chem. Phys. 68 (2001) 22–30.
[28] L.Q. Jing, H.G. Fu, B.Q. Wang, D.J. Wang, B.F. Xin, S.D. Li, J.Z. Sun, Appl. Catal. B 62 (2006) 282–291.
[29] Y. Bessekhouad, D. Robert, J.-V. Weber, J. Photochem. Photobiol. A: Chem. 163 (2004) 569–572.
[30] M. Grätzel, Nature 414 (2001) 338–344.
[31] J. Bai, J. Li, Y. Liu, B. Zhou, W. Cai, Appl. Catal. B: Environ. 95 (2010) 408–413.
[32] S. Banerjee, S.K. Mohapatra, P.P. Das, M. Misra, Chem. Mater. 20 (2008) 6784–6791.
[33] J.S. Jang, S.H. Choi, H.G. Kim, J.S. Lee, J. Phys. Chem. C 112 (2008) 17200–17205.
[34] J.S. Jang, W. Li, S.H. Oh, J.S. Lee, Chem. Phys. Lett. 425 (2006) 278–280.
[35] Y. Tak, S.J. Hong, J.S. Lee, K. Yong, J. Mater. Chem. 19 (2009) 5945–5951.